metals

MDPI

Article

Strength Enhancement of Superduplex Stainless Steel Using Thermomechanical Processing

M. A. Lakhdari [1,2,*], F. Krajcarz [2], J. D. Mithieux [2], H. P. Van Landeghem [1] and M. Veron [1]

[1] Univ. Grenoble Alpes, CNRS, Grenoble INP, SIMAP, F-38000 Grenoble, France; hugo.van-landeghem@grenoble-inp.fr (H.P.V.L.); muriel.veron@grenoble-inp.fr (M.V.)
[2] Aperam Research, rue Roger Salengro, 62330 Isbergues, France; florent.krajcarz@aperam.com (F.K.); jeandenis.mithieux@aperam.com (J.D.M.)
* Correspondence: mohammed_ali-lakhdari@hotmail.com; Tel.: +33-4-7682-6624

Abstract: The impact of microstructure evolution on mechanical properties in superduplex stainless steel UNS S32750 (EN 1.4410) was investigated. To this end, different thermomechanical treatments were carried out in order to obtain clearly distinct duplex microstructures. Optical microscopy and scanning electron microscopy, together with texture measurements, were used to characterize the morphology and the preferred orientations of ferrite and austenite in all microstructures. Additionally, the mechanical properties were assessed by tensile tests with digital image correlation. Phase morphology was not found to significantly affect the mechanical properties and neither were phase volume fractions within 13% of the 50/50 ratio. Austenite texture was the same combined Goss/Brass texture regardless of thermomechanical processing, while ferrite texture was mainly described by α-fiber orientations. Ferrite texture and average phase spacing were found to have a notable effect on mechanical properties. One of the original microstructures of superduplex stainless steel obtained here shows a strength improvement by the order of 120 MPa over the industrial material.

Keywords: superduplex stainless steels; thermomechanical treatment; morphology; texture; mechanical properties

Citation: Lakhdari, M.A.; Krajcarz, F.; Mithieux, J.D.; Van Landeghem, H.P.; Veron, M. Strength Enhancement of Superduplex Stainless Steel Using Thermomechanical Processing. *Metals* **2021**, *11*, 1094. https://doi.org/10.3390/met11071094

Academic Editor: Andrey Belyakov

Received: 1 June 2021
Accepted: 6 July 2021
Published: 9 July 2021

1. Introduction

Among the different types of stainless steel, duplex grades, which are two-phase alloys consisting of equal volume fractions of austenite and ferrite phases in their microstructure, provide the best compromise between mechanical properties and corrosion resistance [1–4]. These materials have attracted great interest due to their outstanding properties, which are desirable in offshore, construction and energy generation applications [1–4]. Superduplex stainless steel is, for instance, the material of choice for offshore rig umbilicals and for heat exchangers in power generation.

As with any other metallic alloy, the mechanical properties of duplex stainless steel (DSS) grades are intimately related to their microstructure [5]. Previous studies [6] proved that thermomechanical processing, which combines heat treatments and rolling, is considered an effective approach to tailor the microstructure of DSS. In the literature, two thermomechanical treatments can be identified: the first, as shown in Figure 1a, is based on an industrial development [7] that consists of a succession of both hot and cold rolling steps followed by annealing. As a result, a strongly oriented microstructure aligned along the rolling direction is obtained.

The second treatment, as described by T. Maki et al. [6], is shown in Figure 1b. It differs from the first process by the application of a solution treatment at high temperature in the ferrite single-phase region after the hot rolling and annealing steps are performed, which leads to the formation of an equiaxed microstructure.

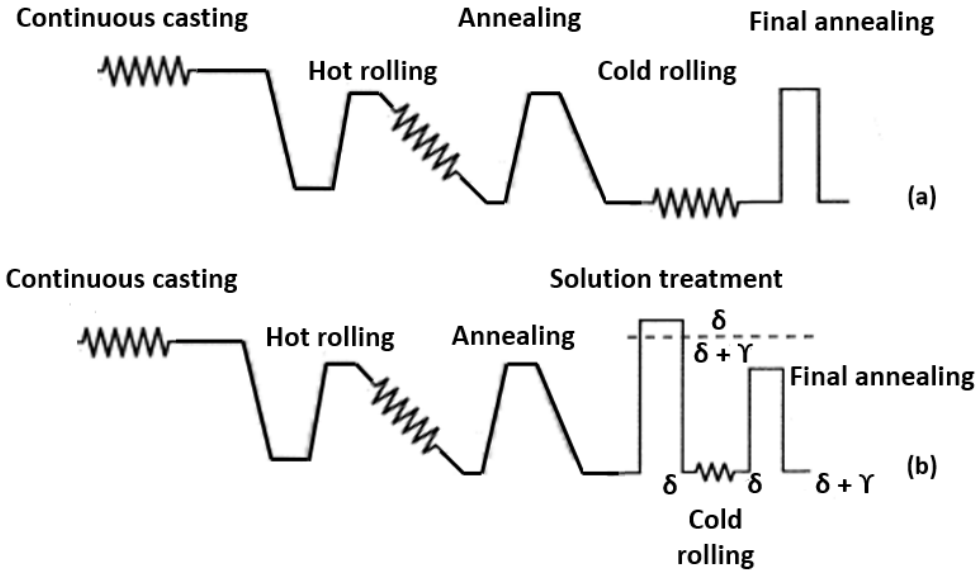

Figure 1. Schematic illustration of the two types of thermomechanical treatments leading to the formation of microduplex structure in duplex stainless steel. (**a**) Industrial processing and (**b**) thermomechanical treatment described by Maki et al. [6].

The mechanical properties of duplex steel 2205 (EN 1.4462) as a function of annealing temperature were investigated by De Lacerda et al. [8]. In this study, duplex steel 2205 was elaborated by industrial processing with three final annealing temperatures: 1060 °C, 1200 °C and 1300 °C. It was shown that the tensile properties decrease as the annealing temperature increases due to the variation of different factors including phase volume fractions, grain size and nitride precipitation. This study did not consider the effects of either morphology or texture evolution.

Two recent studies have been carried out in order to investigate the mechanical properties of superduplex stainless steel as a function of the evolution of its microstructure. In the first work [9], the authors performed several annealing treatments at low temperatures between 400 °C and 600 °C after the hot rolling step. It was shown that the two most influential occurring phenomena are represented by the stress relief and the secondary phase precipitation. In the second one [10], the effect of controlled cold rolling on the microstructure and mechanical properties of the rare earth Ce-modified superduplex stainless steel was investigated. It is shown that with the increase in deformation, the strength of Ce-modified superduplex stainless steel increases rapidly and the elongation decreases dramatically. It should be noted that in both works, the grain morphology is mainly elongated, as well as additional phases besides ferrite and austenite being present.

The textures of the different phases obtained after the thermomechanical processing can be mainly described by a rolling texture that is characteristic of cubic structures [6,11–13]. On one hand, ferrite texture is described by α-fiber orientations and especially by the {100}<011> orientation. On the other hand, austenite texture is described by the Goss ({011}<100>) and Brass ({011}<112>) orientations.

Hutchinson et al. [14], and Komenda and Sandström [15] reported anisotropic tensile properties in duplex structure 2205 produced by rolling. They compared the mechanical responses in different directions in the plane according to their morphologies. It was demonstrated that the observed anisotropy is controlled mainly by the crystallographic texture, while the morphology showed no measurable impact on the overall mechanical response.

However, there are few reports in the literature regarding the relationship between microstructural evolution and mechanical properties in superduplex stainless steel 2507 (EN 1.4410). Those properties are a critical advantage of this alloy in its various applications over competing materials, and it is thus highly desirable to understand how these properties can be tailored, notably through microstructure control. With this in mind, it is

important first to understand the effect of the various microstructural parameters of the alloy on its mechanical properties.

The objective of the present work is to investigate the impact of microstructural evolution on mechanical tensile properties in flat superduplex stainless steel. To this end, samples of the same superduplex stainless grade were treated according to a set of thermomechanical schedules specifically designed to produce clearly distinct microstructures. The crystallography, phase morphology and mechanical properties were thoroughly characterized. The results were analyzed to identify the relationship between the microstructural features and the mechanical properties.

2. Experimental Procedures

2.1. Material

The material used in this study is UNS S32750 superduplex stainless steel, usually known as 2507. It is provided by Aperam as hot-rolled, annealed and pickled (HRAP) plates of 5.5 mm thickness, and cold-rolled (CR) or cold-rolled and annealed (CRA) sheets of 1.5 mm thickness. The chemical composition of the material is given in Table 1.

Table 1. Chemical composition of UNS S32750 superduplex stainless steel (wt %) measured by combustion (infrared absorption for C), combustion (conductimetry for N), and by X-ray fluorescence for the rest.

Fe	Cr	Ni	Mo	Mn	C	N	Other
62	26	7	3.8	0.8	0.017	0.27	<0.051

2.2. Thermomechanical Processing

The base material presented in Section 2.1 is subjected to different thermomechanical schedules in order to produce the five microstructures on which the study is based: the industrial microstructure (IM), the modified annealed microstructures (MAM1 & MAM2), the ultrafine microstructure (UM) and the equiaxed microstructure (EM).

2.2.1. Industrial and Modified Annealed Microstructures

The microstructure obtained by industrial processing is called the industrial microstructure, which corresponds to the microstructure of the final industrial product. As described before, the industrial processing is mainly composed of five steps. The first step is continuous casting, during which superduplex, as with all types of DSS, solidifies in ferrite, followed, in the solid state, by the precipitation of austenite in the form of Widmanstätten patterns. In the 1370–1050 °C range, ferrite (δ) and austenite (γ) are the only thermodynamically stable phases in SDSS. These temperatures are representative of hot-rolling, i.e., conditions under which the lamellar duplex microstructure is obtained through the plastic deformation of Widmanstätten austenite. After first annealing operation aiming at recrystallizing this microstructure, leading to the so-called HRAP state, a cold rolling step with 72% thickness reduction is performed, as shown in Figure 1a, providing the CR state. The last step consists of continuous annealing to recrystallize the two phases of SDSS and to obtain equal volume fractions, corresponding to the CRA microstructure.

From the CR microstructure, modified annealed microstructures are obtained by applying two final annealing conditions. In this study, heat treatments at 1100 °C for 0 s (MAM1) and at 1180 °C for 300 s (MAM2) are carried out on a Gleeble 3500(VPG Brand), as shown in Figure 2. The annealing treatments are carried out in air and with a heating rate of 100 °C/s. To ensure temperature homogeneity, three equidistant thermocouples are used during the annealing treatments, where one is placed on the center of the sample and the two others on both sides. At the end of the treatment, the samples are water cooled to freeze the microstructure.

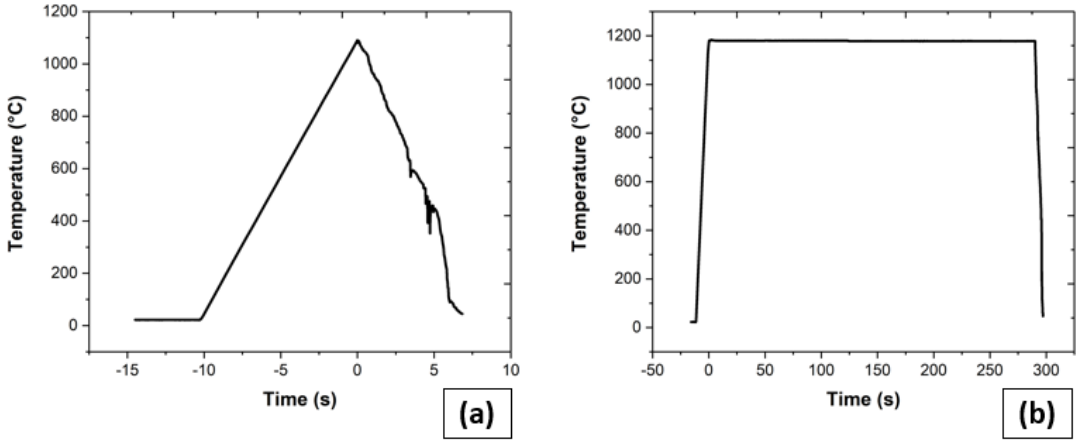

Figure 2. Final annealing treatments carried out on a Gleeble 3500 to obtain modified annealed microstructures at (**a**) 1100 °C for 0 s (MAM1) and at (**b**) 1180 °C for 300 s (MAM2).

2.2.2. Ultrafine and Equiaxed Microstructures

The ultrafine microstructure (UM) is elaborated according to the thermomechanical treatment described by Maki et al. [6]. The main task is to determine the conditions appropriate for a solution treatment and cold rolling in the case of SDSS. As shown in Figure 3a, following the HRAP step, the sample is first solution-treated in the temperature range of the ferrite single-phase region, i.e., above 1370 °C, and water quenched in order to obtain supersaturated ferrite at room temperature. The solution-treated specimen is then cold-rolled with a 90% thickness reduction, and subsequently annealed at 1100 °C for 4 min in the ferrite + austenite two-phased region to recover the duplex microstructure with a phase ratio close to 50/50.

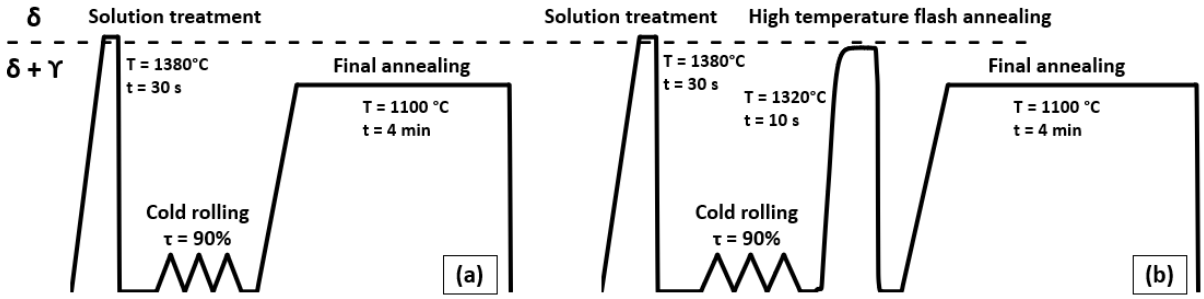

Figure 3. Thermomechanical treatments used to elaborate an (**a**) ultrafine microstructure and (**b**) equiaxed microstructure of superduplex stainless steel 2507.

As shown in Figure 3b, an additional step is added after cold rolling, which consists of a flash annealing treatment at high temperature, 1320 °C, for 10 s, followed by water quenching, resulting in the formation of the equiaxed microstructure.

2.3. Microstructure Characterization

The microstructures resulting from each of the above-listed thermomechanical process are characterized on sheet cross sections (RD-ND).

Samples for light microscopy are first ground with silicon carbide papers from P320 to P2400. They are then polished using diamond pastes with particles of 3 µm then 1 µm. They are finally etched with Beraha's reagent, composed of 0.27g of $K_2S_2O_5$, 20 mL of *HCl* and 100 mL of H_2O, to reveal the two phases of SDSS. This etching leaves ferrite grains in dark and austenite ones in light. The samples are observed using an Olympus DSX500 light microscope.

Electron backscattered diffraction (EBSD, EDAX) in the scanning electron microscope (SEM, Zeiss Ultra 55) is used to determine the crystallographic texture of both phases. In order to improve the specimen surface quality for EBSD analysis, samples were ground and polished, as described for light microscopy, with an additional final step of mechanochemical polishing using colloidal silica in order to remove the residual deformation or stress resulting from mechanical polishing. The acquired EBSD maps are 2 mm long and cover the whole thickness of the sheet samples. They were recorded in a Zeiss Ultra 55 SEM using an EDAX EBSD detector and the following settings: voltage: 20 kV; step size: 150 nm; acquisition speed: 250 fps.

2.4. Morphological Analyses

The aim of morphological analyses is to describe the shape evolution of both phases across the various SDSS microstructures and to determine their volume fraction. In order to carry out this task, the morphological measurements are performed using the public domain programm ImageJ (NIH) and Aphelion software packages(ADCIS, 4.4.0). To do so, light micrographs are binarized using the "Minimum" thresholding method before the surface fractions of phases are measured with ImageJ.

Two parameters are used to characterize the austenite-ferrite microstructure: the mean chord size and weighted average Feret's diameter. The Feret's diameter is weighted using the particle surface areas. The first parameter is measured with the Aphelion software package and the second one with the ImageJ software package. The size of the measuring frame is 4 mm long over the entire thickness. The chord size, which is the length of an object intersection with the test line, is used to measure the characteristic length for both phases of SDSS [15,16]. The measurement of the chord size in the normal direction (ND) is performed by counting the intersections between the particles and the test grid, which consists of an equal number of lines and pixels, determined by the length of the light micrograph. This measurement makes it possible to calculate the layer thickness of both phases of SDSS, as described by the ASTM E1268 standard [17]. Feret's diameter along the rolling and normal directions are used to characterize the austenite particles' length and shape (aspect ratio). To this end, after binarizing the light micrograph, the austenite particles are identified using the "Analyze particle" macro before Feret's diameter is measured by ImageJ.

2.5. Tensile Tests

The mechanical characterization is carried out by tensile tests with image correlation. The experimental device consists of a servo-hydraulic Zwick (ZwickRoell) machine with a CCD camera (6 MPixel) pointing at the area to be observed. The tensile tests are performed in the rolling direction at room temperature, and with displacement control, at a rate of 2 mm/min. Sample elongation is measured with a virtual extensometer using Digital Image Correlation. GOM Correlate 2.0.1 software (GOM GmbH, ZEISS company) is used to process the images taken during the test. The uniaxial tensile tests use rectangular cross-section samples machined by electrical discharge machining to minimize plastic deformation. Their dimensions comply with ASTM 8 [18] (length = 12.5 mm, width = 3.1 mm, l/w = 4) with thickness that varies between 0.5 and 1.5 mm. For each microstructure, five to seven tensile tests are performed in order to ensure the reproducibility of their strength properties.

3. Results

3.1. Microstructure Evolution

The industrial microstructure and modified annealed microstructures are strongly oriented and aligned with the rolling direction, as shown in Figure 4. This morphology results from the rolling processes.

A characteristic pancake microstructure is observed, consisting of flattened, widened and elongated ferrite and austenite bands, whose mean thickness (dimension in ND) is between 2 and 4 μm. Figure 5 presents the grain maps for the industrial microstructure.

It should be noted that the ferrite and austenite layers in microstructures of this type are essentially one grain thick, which makes it possible to consider the layer spacing in ND as a good approximation of the grain size.

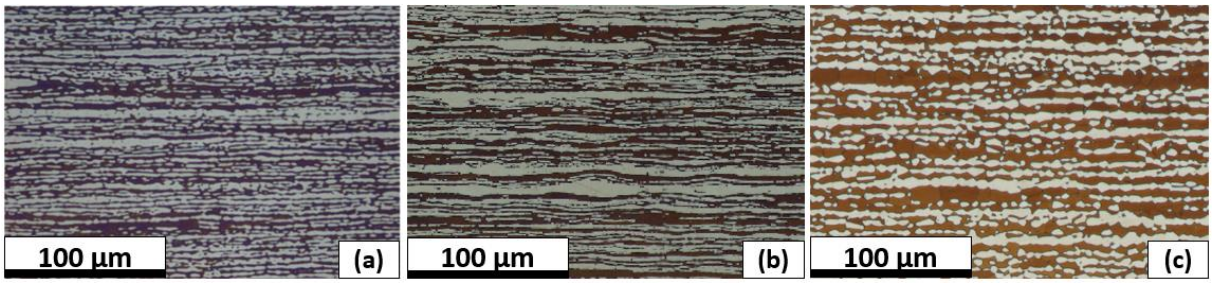

Figure 4. Industrial (**a**) and modified annealed (**b**) 1100 °C—0 s and (**c**) 1180 °C—300 s microstructures where ferrite grains appear in dark and austenite ones in light.

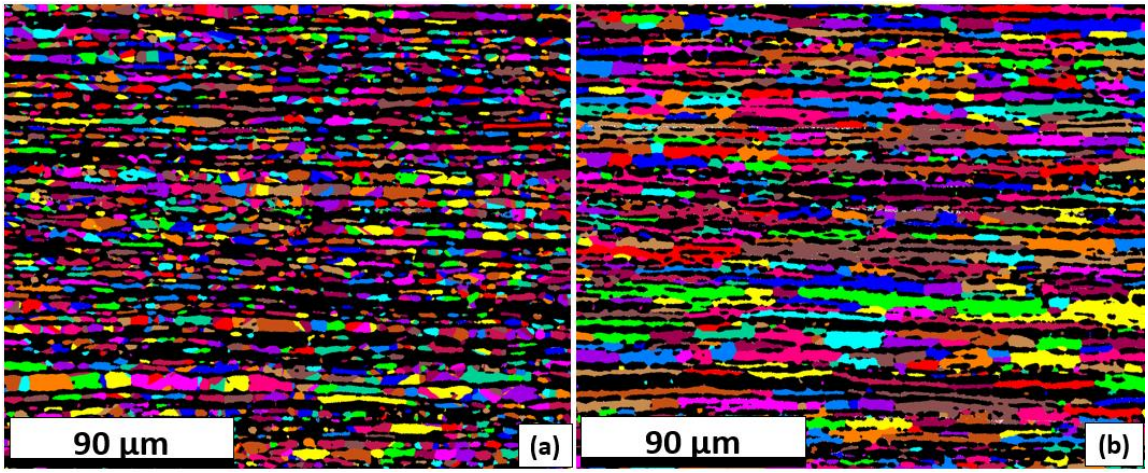

Figure 5. (**a**) Ferrite and (**b**) austenite grain maps of the industrial microstructure with a minimum misorientation of 15°.

The main differences between these three microstructures are the lengths of austenite layers, the thickness of ferrite layers and the phase volume fractions. As reported in Table 2, an increase in the ferrite volume fraction and ferrite layers' thickness by 13% and 100%, respectively, and a decrease in the austenite layers' length by 91% are observed with increasing of the annealing conditions. This evolution is governed by thermodynamic considerations and the surface energies of the interfaces and grain boundaries [19].

In the case of the ultrafine microstructure shown in Figure 6, austenite particles in the form of relatively short bands are precipitated along and within ferrite grains, as shown in Figure 6. As in previous cases, and as can be noticed in Figure 6, they are oriented along the rolling direction and are one grain thick. Morphological measurements in ND show that the mean thickness, taken as the mean chord size along ND, is about 2 µm. Furthermore, the mean length of austenite particles measured in the rolling direction is about 40 µm.

From Figure 7, the comparison between ferrite grain maps with minimum misorientation of 5° and 15° reveals a structure of subgrains in the ferrite matrix. In addition, it can be seen that the ferrite matrix grains are much larger, about a hundred times, than in the industrial microstructure.

Table 2. Microstructures morphological characteristics of superduplex stainless steel.

Parameters	Industrial Microstructure	Modified Annealed (1100 °C—0 s)	Modified Annealed (1180 °C—300 s)	Ultrafine Microstructure	Equiaxed Microstructure
Ferrite volume fraction	50% ± 1%	49% ± 1%	62% ± 1%	50% ± 1%	50% ± 1%
Mean Chord size in ND (ferrite)	2.4 ± 0.2 µm	2.0 ± 0.2 µm	4.0 ± 0.2 µm	2.3 ± 0.2 µm	5.1 ± 0.2 µm
Mean chord size in ND (austenite)	2.3 ± 0.2 µm	2.1 ± 0.2 µm	2.6 ± 0.2 µm	2.0 ± 0.2 µm	5.0 ± 0.2 µm
Feret's diameter in RD	291 ± 5 µm	1633 ± 58 µm	140 ± 1 µm	39.4 ± 0.4 µm	46.0 ± 0.2 µm
Aspect ratio	18 ± 1	25 ± 1	15 ± 1	3.3 ± 0.7	2.3 ± 0.1

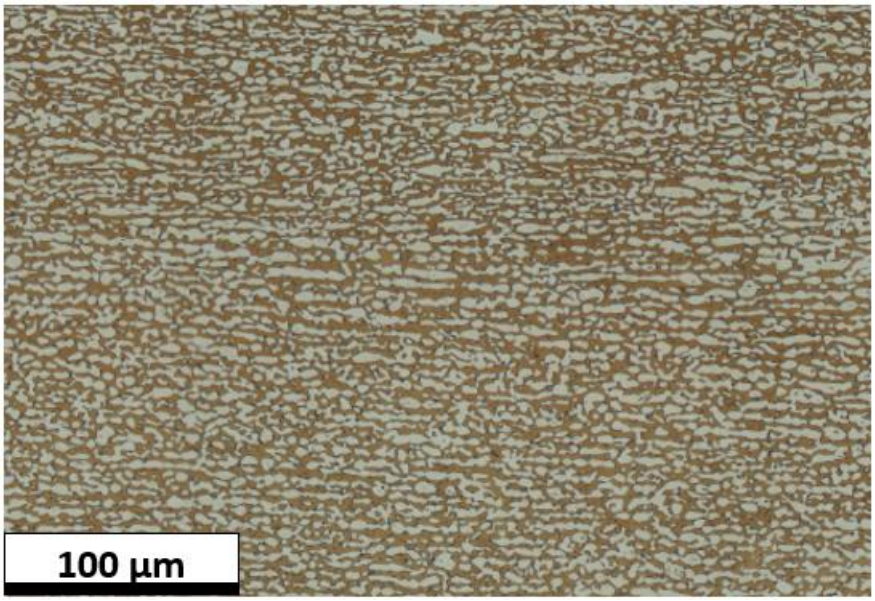

Figure 6. Ultrafine microstructure of superduplex stainless steel. Ferrite grains appear in dark and austenite ones appear in light.

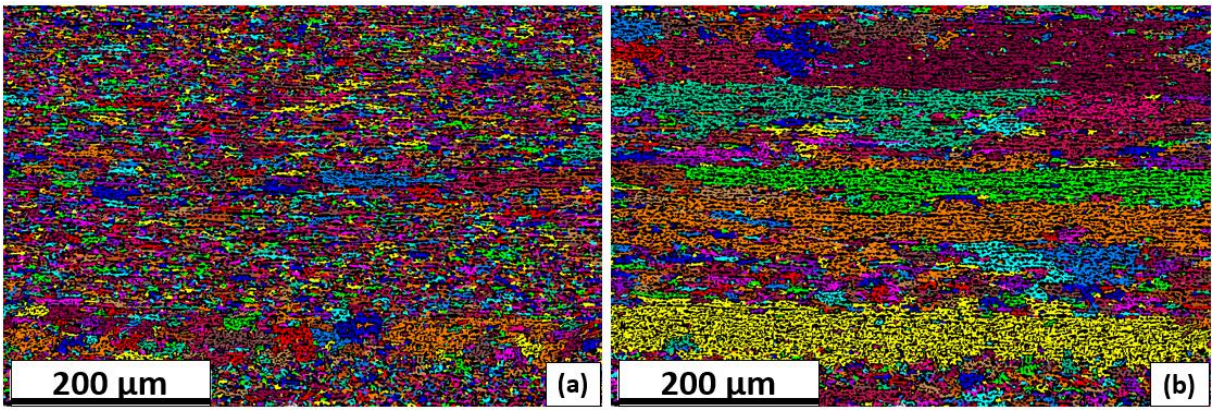

Figure 7. Ferrite grain maps with minimum misorientation of (**a**) 5° and (**b**) 15° of the ultrafine microstructure.

In order to obtain an equiaxed microstructure of SDSS, it proved necessary to modify the thermomechanical treatment described by Maki et al. [6]. For this reason, a flash

annealing treatment at high temperature is added after the cold rolling step. The resulting microstructure is illustrated in Figure 8, where austenite particles in the form of equiaxed grains are precipitated in the ferrite matrix. Morphological measurements show that the mean length of austenite particles is about 45 µm and the mean chord size in ND measured is about 5 µm.

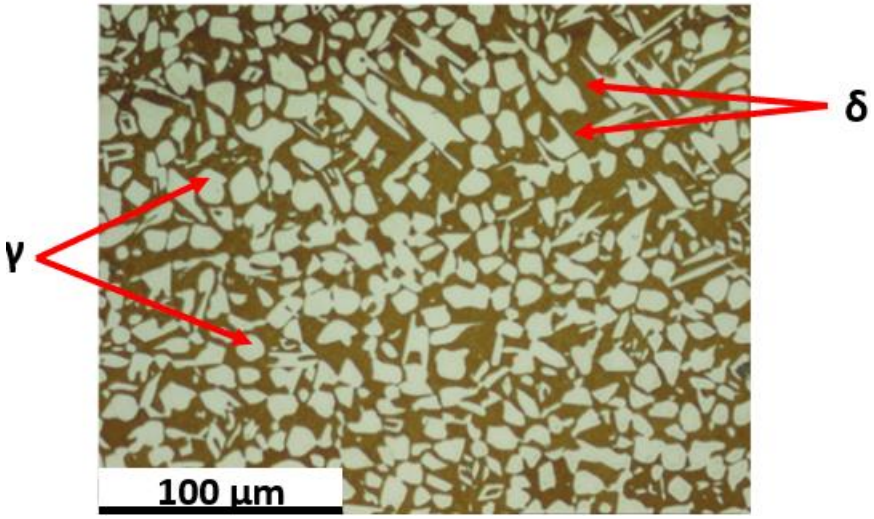

Figure 8. Equiaxed microstructure of superduplex stainless steel. Ferrite grains appear in dark and austenite ones appear in light.

The ferrite matrix grains, as presented in Figure 9b, have a size similar to those of the ultrafine microstructure but with a more equiaxed morphology. Contrary to the ultrafine case, however, there are much fewer differences between ferrite grain maps, presented in Figure 9, with minimum misorientations of 5° and 15°.

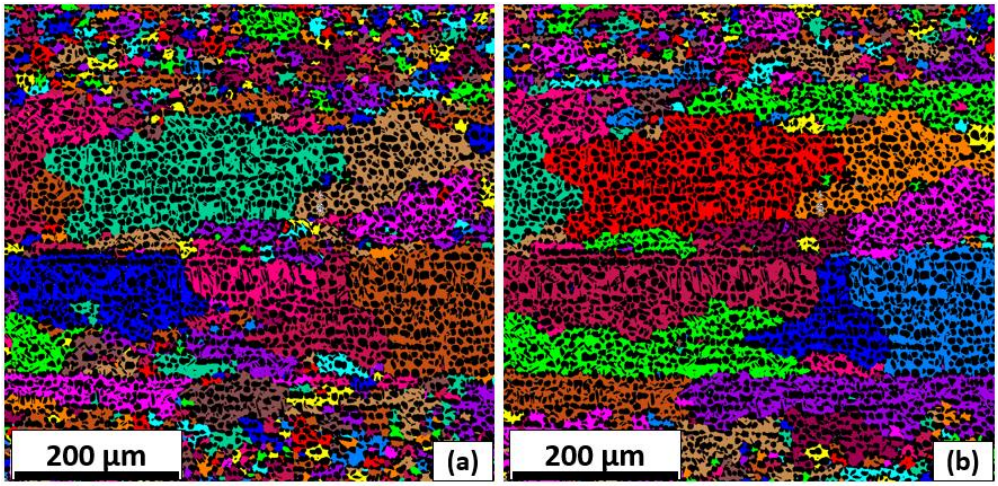

Figure 9. Ferrite grain maps with minimum misorientations of (**a**) 5° and (**b**) 15° of the equiaxed microstructure.

3.2. Texture Evolution

The textures of ferritic and austenitic phases in three microstructures of SDSS—industrial, ultrafine and equiaxed microstructures—are presented in Figures 10 and 11. It should be noted that the texture of modified annealed is not shown here as it is highly similar to that of the industrial microstructure. Textures appear with a marked intensity in ferrite, mainly described by α-fiber (<110>//RD) spread from {001}<110> to {112}<110>. Ferrite textures along α-fiber show a maximum on {001}<110> in the industrial microstruc-

ture and on {011}<011>, {112}<110> in the equiaxed microstructure. An interesting feature is the weakness of {111}<110> in the case of all the components of the γ-fiber, which are normally the dominating textures for BCC structures after rolling and annealing [6,12]. In the case of ultrafine microstructure, ferrite presents strong {001}<110> and {111}<011> textures.

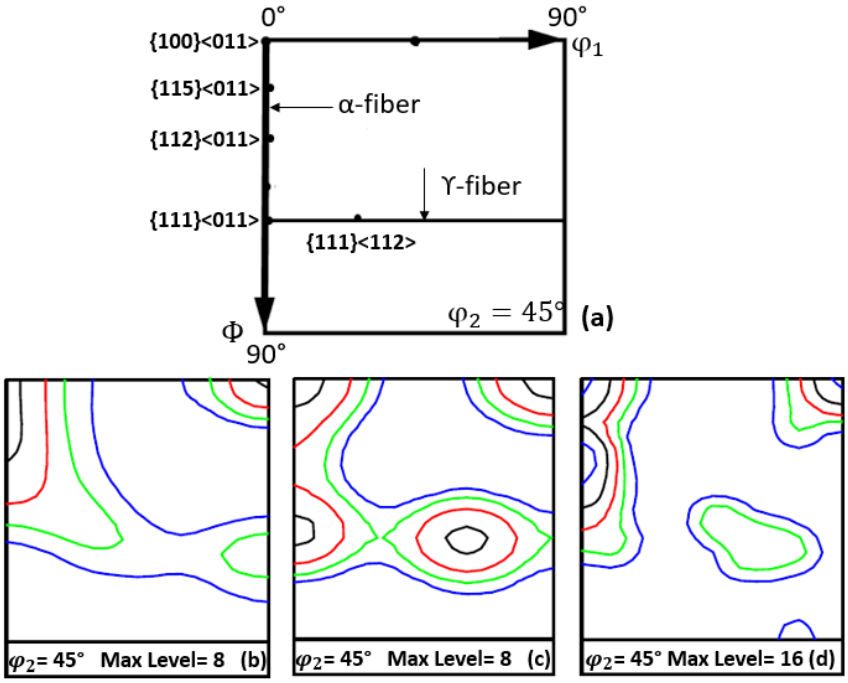

Figure 10. (**a**) Orientation distribution function section with select fibers and orientations in BCC metals. Ferrite textures of superduplex stainless steel are presented in the same section for the (**b**) industrial, (**c**) ultrafine and (**d**) equiaxed microstructures.

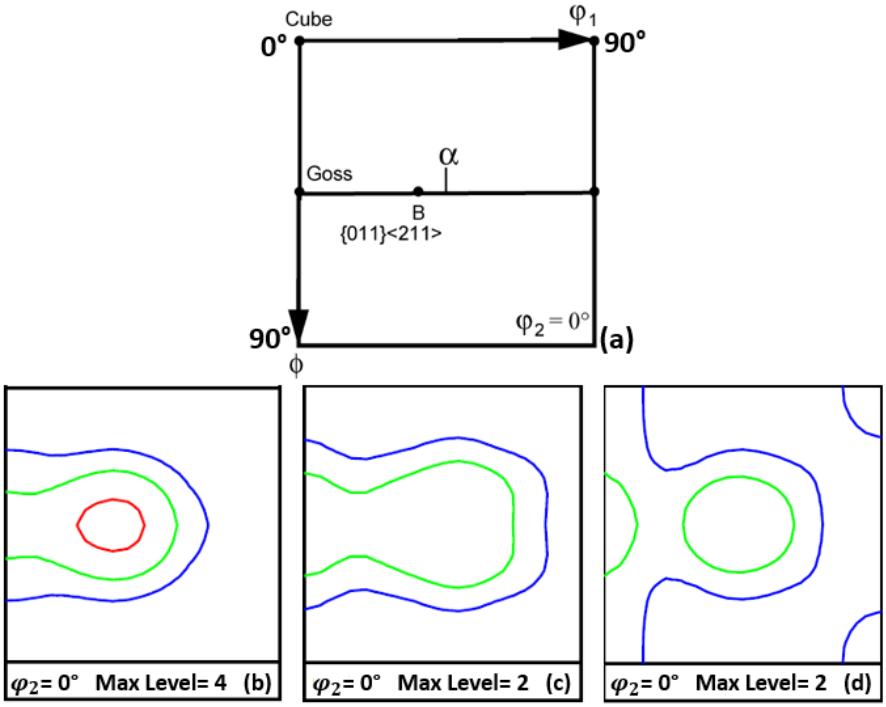

Figure 11. (**a**) Orientation distribution function section with select fibers and orientations in FCC metals. Austenite textures of superduplex stainless steel are presented in the same section for the (**b**) industrial, (**c**) ultrafine and (**d**) equiaxed microstructures.

Austenite textures in all microstructures of SDSS, as shown in Figure 11, are mainly described by Brass {011}<211> and Goss {011}<100> orientations. These results are in agreement with previous studies carried out on duplex stainless steels [7,14].

3.3. Mechanical Properties

Mechanical properties for all microstructures of SDSS are characterized by uniaxial tensile test with digital image correlation. Figure 12 shows the true stress–strain curves obtained for the different microstructures of the study. The main mechanical properties obtained from the engineering stress–strain curves are presented in Table 3.

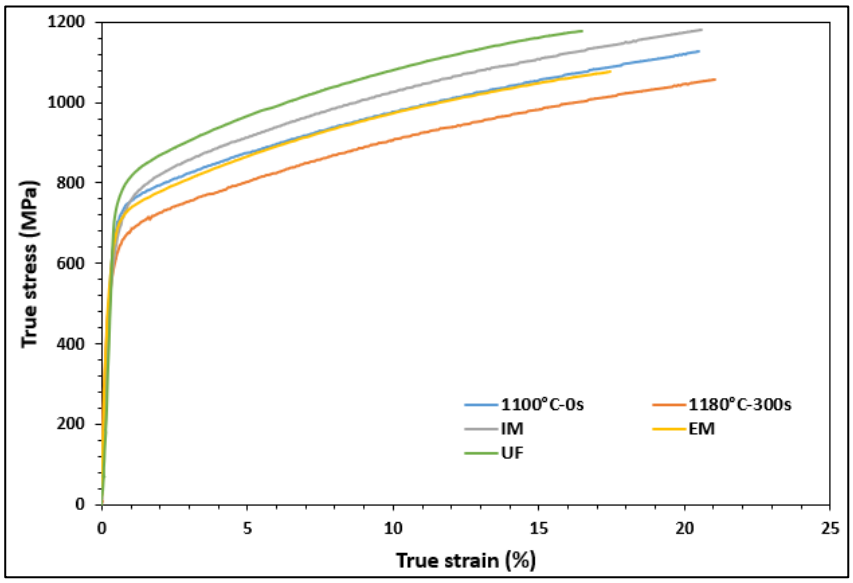

Figure 12. Tensile true stress–strain curves for all microstructures of superduplex stainless steel.

Table 3. Tensile mechanical properties for all microstructures of superduplex stainless steel 2507. σ_{YS}: Offset yield stress; σ_{UTS}: Ultimate tensile stress; ε: Uniform elongation.

Parameters	Annealed State (1100 °C—0 s)	Annealed State (1180 °C—300 s)	Industrial Microstructure	Ultrafine Microstructure	Equiaxed Microstructure
σ_{YS} (MPa)	710 ± 13	643 ± 3	653 ± 7	772 ± 13	695 ± 8
σ_{UTS} (MPa)	920 ± 10	857 ± 7	952 ± 12	1000 ± 5	918 ± 15
ε (%)	20 ± 0.9	22.5 ± 0.9	20.2 ± 0.9	16.5 ± 1.6	17.7 ± 0.2

Mechanical properties of the industrial microstructure are characterized by a yield stress (ε = 0.2%) and an ultimate tensile stress of the order of 650 and 950 MPa, with a uniform elongation of the order of 22.5%. In comparison with other microstructures, the mechanical behavior of industrial microstructure is bounded at the top by that of ultrafine microstructure and at the bottom by that of equiaxed microstructure and modified annealed microstructure.

The comparison between industrial, ultrafine and equiaxed microstructures in terms of mechanical properties shows a maximal difference of about 120 MPa regarding yield stress, 80 MPa regarding ultimate tensile strength and 3.7% regarding uniform elongation. In the case of modified annealed microstructure, the strength properties decrease as the annealing conditions, time and temperature increase.

4. Discussion

The different microstructures elaborated in this study by thermomechanical treatments show that in the case of SDSS, the implementation of the thermomechanical processing

described by Maki et al. [6] does not allow the obtaining of an equiaxed microstructure. In fact, the resulting microstructure is characterized by austenite particles that are oriented along the rolling direction. This remarkable change can be attributed to the presence of austenite after solution-treatment, as shown in Figure 13, where the austenite volume fraction measured at the skin and at the core are 2% and 30% ± 1%, respectively. This amount of austenite is related to the quenching rate, which is controlled by the heat diffusion through the thickness. On the other hand, it is worth noting that this amount is the smallest amount possible given the capabilities of the heat treatment facilities used for the solution treatments of the present study.

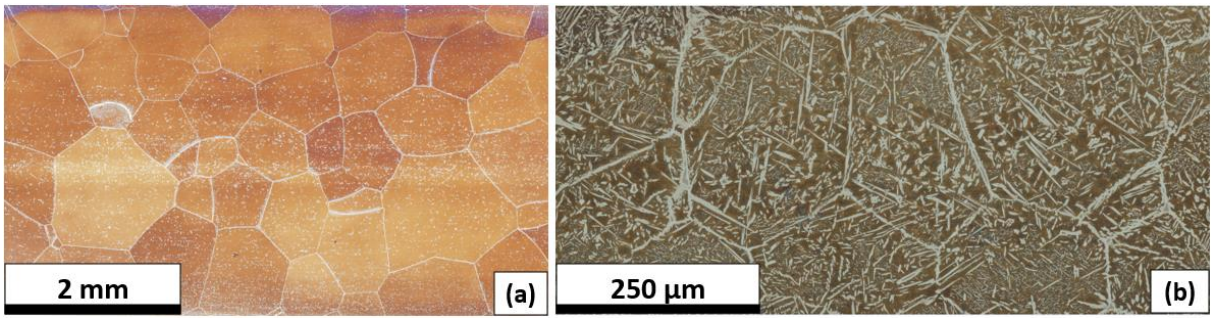

Figure 13. Microstructures of (**a**) the skin and (**b**) the core of a solution-treated sample. Ferrite grains appear in dark and austenite ones appear in light.

The results of EBSD analyses show that in the case of microstructures obtained through the industrial process shown in Figure 5, ferrite grain size is similar to that of austenite. In the case of ultrafine and equiaxed microstructures, ferrite grain size is much larger than that of austenite, as shown in Figures 7b and 9b. This difference is introduced by the solution and flash-annealing steps, during which the absence of austenite enables rapid growth of ferrite grains. The large difference in ferrite grain sizes observed between these two groups of microstructures highlights the effectiveness of the duplex structure at inhibiting grain growth.

During final annealing, the elastic energy stored in the material due to the plastic deformation from cold rolling leads to the recrystallization of both phases of the industrial microstructure. This is illustrated in the case of ferrite by the grain maps where changing the minimum misorientation between grains from 5° to 15° changes little.

In the case of ultrafine microstructure, the EBSD observations presented in Figure 7 reveal a structure of subgrains in ferrite formed by recovery. As for austenite, which has a low SFE [12,13], grains have been recrystallized. It is interesting to note that, despite the cold-rolling reduction in the ultrafine microstructure (90%) being larger than that of the industrial microstructure (72%), the ferrite of the former was recovered, while that of the latter was recrystallized during the final annealing treatment, which was carried out under the same conditions in both cases. This observation is justified by a pinning effect due to austenite particles [6]. In fact, during the final annealing treatment in the case of the ultrafine microstructure, it is characteristic that the recovery of deformed ferrite matrix occurs rapidly and the subgrain structure of ferrite matrix is formed readily prior to the precipitation of austenite phase in the earliest stage of aging. By further holding at 1100 °C, the volume fraction of austenite is increased to about 50%. The precipitation of austenite particles, which preferentially occurred in the subgrain structure, prevents the migration of ferrite subgrain boundaries and, consequently, the recrystallization of ferrite.

Unlike ultrafine microstructure, the two phases of equiaxed microstructure are recrystallized. In the case of ferrite, this is illustrated by the grain maps shown in Figure 9, where changing the minimum misorientation between grains from 5° to 15° changes little. This outcome is due to the flash annealing treatment at 1320 °C where the recrystallization of ferrite occurs in the absence of austenite precipitation. Another consequence of the

flash annealing treatment is that the precipitation of austenite during the final annealing treatment occurs in a recrystallized ferritic microstructure, which leads to the obtaining of an equiaxed morphology.

It is already known in the literature [11,12] that, on the one hand, in the case of ferritic materials, the recovery texture is described by deformation orientations which are α-fiber orientations, especially {100}<011> and {112}<011>, while recrystallization texture is described by γ-fiber orientations, especially {111}<112>. On the other hand, austenitic materials are likely to recrystallize and, as a result, they develop a particular Brass Recrystallization orientation {236}<385>. In this study, and from the orientation distribution functions shown in Figures 10 and 11, it can be seen that regardless of the outcome of the competition between recovery and recrystallization, the textures are mainly described by deformation orientations in all conditions. In fact, the ferrite texture in all microstructures of SDSS is mainly described by α-fiber orientations, and one can notice the absence of the Brass Recrystallization orientation in recrystallized austenite. All in all, this finding means that the duplex structure influences the development of the phase textures. As suggested in [12], texture development in austenite during annealing may be attributed to oriented nucleation or strain induced boundary migration, which leads to recrystallization textures similar to the deformation textures.

From tensile tests shown in Figure 12, differences in mechanical properties between the microstructures of SDSS can be observed. In the following, an attempt is made to relate these differences to the microstructural parameters that were observed to vary across the microstructures, including austenite particle morphology, phase volume fraction, grain size and texture.

The effect of morphology can be identified by comparing ultrafine and industrial microstructures. As reported in Table 3, the strength properties of the former are higher than those of the latter. This outcome, associated with the fact that the aspect ratio value reported in Table 2 is much lower in the case of ultrafine than industrial microstructure, suggests that the phase morphology of SDSS has no effect on its overall mechanical response. Indeed, according to the Shear-lag theory [20], the flow stress of the composite (σ_f) is given in the form of:

$$\sigma_f = \sigma_\alpha + \frac{L}{2d}\,\sigma_\alpha\,V \tag{1}$$

where σ_α is the flow stress of the matrix, and V and $\frac{L}{d}$ are the volume fraction and the aspect ratio of the second phase. Based on Equation (1), a higher value of flow stress is expected in the industrial microstructure rather than in the ultrafine microstructure if phase morphology has an effect on mechanical properties in SDSS. This result is in agreement with previous works [14,16] carried out on rolled duplex stainless steels, which show that the phase morphology has no effect on their mechanical properties.

It is already shown in duplex steels that ferrite is the resistant phase at the beginning of plasticity at room temperature [21,22]. Consequently, a larger ferrite volume fraction would be expected to result in a higher yield stress. Among the microstructures studied here, a maximum difference in ferrite fraction of 13% is found between the samples annealed for 0 s at 1100 °C and for 300 s at 1180 °C. However, it is found that the former, containing less ferrite, is stronger than the latter. This suggests that limited variations around the 50/50 phase fractions characteristic of DSSs have a negligible effect on mechanical properties compared to grain size and texture.

The difference in strength properties between modified annealed microstructures, which is about 70 MPa, can mainly attributed to grain size effect. It can be seen from this comparison that the grain size has an important effect on strength properties of SDSS, even with small variation. This result could be understood by the small grain size due to the duplex structure on one side, and the high Hall–Petch coefficient of ferrite and austenite materials on the other side. In fact, it is reported in the literature that the Hall–Petch ($MPa.\,mm^{-0.5}$) coefficient of ferritic steel is of the order of tens [23,24]. In austenitic material, it is less than ten, which is clearly low compared to the Hall–Petch coefficient of

ferritic steel. However, the study carried out by Norström [25] on the influence of nitrogen and grain size on yield stress in 316L austenitic stainless steel shows that the total effect of nitrogen on yield strength is composed of two different contributions: one independent of grain size and the other markedly dependent upon it. As seen in Table 1, SDSS 2507 contains a significant amount of nitrogen that should lead to austenite contents in excess of 0.5wt %. In fact, based on the Norström equation, the expected hardening according to grain size in austenite should be of the order of 550 MPa in terms of nitrogen concentration in SDSS, which is six times higher than without it. This value is an extrapolation, as Norström's coefficient was determined for much lower nitrogen contents, and should, therefore, be used with caution. However, it does reveal the strong synergy between austenite grain size and nitrogen content. However, comparing the 1180 °C—30 s modified annealed microstructure with the slightly coarser equiaxed microstructure shows that the latter is stronger, indicating that, on the one hand, the approximation of grain size in coarser microstructures by average phase spacing, which is measured by chord size, is a good way to characterize the size effect. On the other hand, it is clear that at least one other factor measurably influences the mechanical properties, and potentially more so than the microstructure size.

Texture characterization of all samples shows that on the one hand, the texture of austenite, which is described by the Goss and Brass orientations, is the same in all microstructures. On the other hand, the main difference in ferrite texture lies in the intensity of the α-fiber and {111}<011> orientation. As presented in Table 2, the ultrafine and the 1100 °C—0 s modified annealed microstructures show almost the same characteristic sizes, but the former is noticeably stronger, as shown in Figure 12. It was noted from Figure 10 that the ferrite textures of these two microstructures are markedly different, notably with a strong {111}<011> component in the ultrafine case that is entirely absent from the industrial and modified annealed microstructures. Major ferrite texture differences can also be noted in the above-mentioned case of the 1180 °C—30 s modified annealed microstructure and the equiaxed microstructure. Again, in these cases, the {111}<011> component is found in the stronger material, although far less so than in the ultrafine case. The equiaxed microstructure also shows a stronger {112}<011> component than that in the industrial and modified cases.

Critical resolved stress shear (CRSS) calculations for ferrite oriented as {100}<011>, {112}<011> and as {111}<011> show that the active slip systems present similar Schmid factors in both cases. This implies that it is not ferrite texture alone but its varying interaction with austenite that leads to pronounced changes in mechanical properties, as suggested by Hutchinson et al. [14].

Finally, it is worth noting that differences in the microstructural features of SDSS, induced by thermomechanical processing, can lead to a strength improvement of the order of 120 MPa over the industrial microstructure. The associated loss in ductility remains limited, with a minimum uniform elongation of 16.5%.

5. Conclusions

The effect of microstructural evolution on mechanical properties was investigated in superduplex stainless steel UNS S32750.

In order to modify the microstructure of SDSS, three main thermomechanical schedules were carried out to generate different morphologies ranging from banded to equiaxed.

In all conditions, austenite was recrystallized and showed a combined Brass/Goss texture. Ferrite was either recrystallized or recovered and displayed a texture with α and γ fibers of varying intensities. The main difference in ferrite texture lies in the intensity of the two orientations, {100}<011> and {111}<011>.

The studied SDSS microstructures have clearly different morphologies. In particular, the aspect ratio values for austenite particles vary between 2 and 25. Despite these significant morphological differences, the average phase spacing of all microstructures measured is less than 5 μm.

It was observed that the insertion of a high-temperature annealing step in the thermomechanical schedule, where the austenite volume fraction is reduced to a few percent, leads to a large ferrite grain size. The large difference between the materials where the austenite fraction remained high and those where it was almost entirely dissolved highlights the effectiveness of the duplex structure in the inhibition of grain growth.

Comparison of the mechanical properties of the different microstructures revealed that the two microstructural parameters that have the strongest effect on tensile strength are ferrite texture and average phase spacing.

One of the original microstructures of SDSS obtained here showed enhanced strength compared to the industrial material with limited ductility loss, suggesting that SDSS thermomechanical processing can be tuned to tailor the properties of the resulting material.

Author Contributions: Conceptualization, M.A.L.; methodology, M.A.L.; software, M.A.L.; validation, M.A.L.; formal analysis, M.A.L.; investigation, M.A.L.; resources, F.K., J.D.M.; data curation, M.A.L.; writing-original draft preparation, M.A.L.; writing-review and editing, F.K., J.D.M., H.P.V.L. and M.V.; visualization, M.A.L.; supervision, F.K., J.D.M., H.P.V.L. and M.V.; project administration, F.K., J.D.M., H.P.V.L. and M.V.; funding acquisition, F.K., J.D.M., H.P.V.L. and M.V.; All authors have read and agreed to the published version of the manuscript.

Funding: The article is: ANRT-CIFRE 2016/1333. Part of this work was performed with the support of the Center of Excellence of Multifunctional Architectured Materials "CEMAM" No. AN-10-LABX-44-01 funded by the "Investment for the Future" Program operated by the National Research Agency (ANR).

Institutional Review Board Statement: Not applicable.

Informed Consent Statement: Not applicable.

Data Availability Statement: Data available on request. The data presented in this study are available on request from the corresponding author.

Conflicts of Interest: The authors declare no conflict of interest.

References

1. Charles, J. Duplex families and applications: A review Part 1: From Duplex Pioneers up to 1991. In Proceedings of the 10th China Iron and Steel Annual Conference and the 6th Baosteel Academic Annual Conference, Shanghai, China, 21–23 October 2015.
2. Charles, J. Duplex families and applications: A review Part 3: The lean duplex grades. In Proceedings of the 10th China Iron and Steel Annual Conference and the 6th Baosteel Academic Annual Conference, Shanghai, China, 21–23 October 2015.
3. Charles, J. Duplex Stainless Steels—A Review after DSS 07 held in Grado. *Steel Res. Int.* **2008**, *79*, 455–465. [CrossRef]
4. Nilsson, J.-O. Super duplex stainless steels. *Mater. Sci. Technol.* **1992**, *8*, 685–700. [CrossRef]
5. Deschamps, A. Microstructure—Properties relationships in metal-based alloys. *WORLD Sci.* **2010**, 73–124. [CrossRef]
6. Maki, T.; Furuhara, T.; Tsuzaki, K. Microstructure development by thermomechanical processing in duplex stainless steel. *ISIJ Int.* **2001**, *41*, 571–579. [CrossRef]
7. Fargas, G.; Akdut, N.; Anglada, M.; Mateo, A. Microstructural Evolution during Industrial Rolling of a Duplex Stainless Steel. *ISIJ Int.* **2008**, *48*, 1596–1602. [CrossRef]
8. de Lacerda, J.C.; Cândido, L.C.; Godefroid, L.B. Effect of volume fraction of phases and precipitates on the mechanical behavior of UNS S31803 duplex stainless steel. *Int. J. Fatigue* **2015**, *74*, 81–87. [CrossRef]
9. Zhou, T. Controlled cold rolling effect on microstructure and mechanical properties of Ce-modified SAF 2507 super duplex stainless steel. *Mater. Sci.* **2019**, *766*, 138352. [CrossRef]
10. Cojocaru, E.M.; Raducanu, D.; Nocivin, A.; Cinca, I.; Vintila, A.N.; Serban, N.; Angelescu, M.L.; Cojocaru, V.D. Influence of Aging Treatment on Microstructure and Tensile Properties of a Hot Deformed UNS S32750 Super Duplex Stainless Steel (SDSS) Alloy. *Metals* **2020**, *10*, 353. [CrossRef]
11. Keichel, J.; Foct, J.; Gottstein, G. Deformation and annealing behavior of nitrogen alloyed duplex stainless steels. Part I: Rolling. *ISIJ Int.* **2003**, *43*, 1781–1787. [CrossRef]
12. Keichel, J.; Foct, J.; Gottstein, G. Deformation and annealing behavior of nitrogen alloyed duplex stainless steels. Part II: Annealing. *ISIJ Int.* **2003**, *43*, 1788–1794. [CrossRef]
13. Fargas, G.; Akdut, N.; Anglada, M.; Mateo, A. Reduction of Anisotropy in Cold-Rolled Duplex Stainless Steel Sheets by Using Sigma Phase Transformation. *Metall. Mater. Trans. A* **2011**, *42*, 3472–3483. [CrossRef]
14. Hutchinson, W.B.; Ushioda, K.; Runnsjö, G. Anisotropy of tensile behaviour in a duplex stainless steel sheet. *Mater. Sci. Technol.* **1985**, *1*, 728–736. [CrossRef]

15. Komenda, J.; Sandström, R. Assessment of pearlite banding using automatic image analysis: Application to hydrogen-induced cracking. *Mater. Charact.* **1993**, *31*, 143–153. [CrossRef]
16. Komenda, J.; Sandström, R. Automatic assessment of a two-phase structure in the duplex stainless-steel SAF 2205. *Mater. Charact.* **1993**, *31*, 155–165. [CrossRef]
17. E04 Committee. *Practice for Assessing the Degree of Banding or Orientation of Microstructures*; ASTM International: West Conshohocken, PA, USA, 2007.
18. E28 Committee. *Test Methods for Tension Testing of Metallic Materials*; ASTM International: West Conshohocken, PA, USA, 2011.
19. Tresallet, D. Evolution des Microstructures au Cours d'un Recuit Dans un Acier Inoxydable Superduplex: Caractérisation et Modélisation. Ph.D. Thesis, Université Grenoble Alpes, Saint-Martin-d'Hères, France, 2019.
20. Cho, K.; Gurland, J. The law of mixtures applied to the plastic deformation of two- phase alloys of coarse microstructures. *Metall. Trans. A* **1988**, *19*, 2027–2040. [CrossRef]
21. Fréchard, S.; Martin, F.; Clément, C.; Cousty, J. AFM and EBSD combined studies of plastic deformation in a duplex stainless steel. *Mater. Sci. Eng. A* **2006**, *418*, 312–319. [CrossRef]
22. David, C. *Influence de la Déformation Plastique sur la Résistance à la Corrosion de L'acier Inoxydable Lean Duplex UNS S32304*; Université Grenoble Alpes: Saint-Martin-d'Hères, France, 2018.
23. Takaki, S. Influence of Alloying Elements on the Hall-Petch Coefficient in Ferritic Steel. *Mater. Sci. Forum* **2012**, *706–709*, 181–185. [CrossRef]
24. Takaki, S. Review on the Hall-Petch Relation in Ferritic Steel. *Mater. Sci. Forum* **2010**, *654–656*, 11–16. [CrossRef]
25. Norström, L.-Å. The influence of nitrogen and grain size on yield strength in Type AISI 316L austenitic stainless steel. *Met. Sci.* **1977**, *11*, 208–212. [CrossRef]